Superconductivity in compounds of sodium-intercalated graphite

Chun-Mei Hao,[1,2] Xing Li,[2] Artem R. Oganov,[3] Jingyu Hou,[4] Shicong Ding,[2] Yanfeng Ge,[2] Lin Wang,[1,2] Xiao Dong,[4] Hui-Tian Wang,[5] Guochun Yang,[2,*] Xiang-Feng Zhou,[1,2,4,†] and Yongjun Tian[1]

[1]*Center for High Pressure Science, State Key Laboratory of Metastable Materials Science and Technology, Yanshan University, Qinhuangdao 066004, China*
[2]*Key Laboratory for Microstructural Material Physics of Hebei Province, School of Science, Yanshan University, Qinhuangdao 066004, China*
[3]*Skolkovo Institute of Science and Technology, Bolshoy Boulevard 30, bld. 1, Moscow 121205, Russia*
[4]*Key Laboratory of Weak-Light Nonlinear Photonics, School of Physics, Nankai University, Tianjin 300071, China*
[5]*National Laboratory of Solid State Microstructures, School of Physics, and Collaborative Innovation Center of Advanced Microstructures, Nanjing University, Nanjing 210093, China*

(Received 22 March 2023; revised 12 November 2023; accepted 15 November 2023; published 5 December 2023)

The discovery of superconductivity in CaC_6 with a critical temperature (T_c) of 11.5 K reignited much interest in exploring high-temperature superconductivity in graphite intercalation compounds (GICs). Here we identify a GIC NaC_4, discovered by *ab initio* evolutionary structure search, as a superconductor with a computed T_c of 41.2 K at 5 GPa. This value is eight times higher than that of the synthesized GIC NaC_2 and possesses the highest T_c among available GICs. The remarkable superconductivity of GIC NaC_4 mainly arises from the coupling of π electrons in graphene with the low-frequency vibrations involving both Na and C atoms. These findings suggest that Na GICs may hold great promise as high-T_c superconductors.

DOI: 10.1103/PhysRevB.108.214507

I. INTRODUCTION

The search for high-temperature superconductors and the discovery of their origins are ongoing topics in condensed matter physics [1–3]. Bardeen-Cooper-Schrieffer (BCS) theory allows one to calculate properties of conventional superconductors. Compounds made of light elements usually have a high Debye temperature, which favors high-temperature superconductivity [4,5]. Thus far, pressurized hydrides, have demonstrated remarkably high critical temperatures (T_cs) that approach room temperature [6,7]. However, maintaining their superconductivity requires extremely high pressure of ~150 GPa or more [8,9], which presents strict requirements for scientific instruments and precludes practical applications. In this regard, the discovery of high-T_c superconductors stabilized at low or even ambient pressure is the next recognized target [10,11].

Carbon is the sixth element in the periodic table and has a low atomic mass. Carbon forms the richest variety of allotropes and compounds among the light elements due to diverse hybridizations (e.g., sp, sp^2, and sp^3) [12–14]. An intriguing feature is that some carbon-based materials synthesized at high temperatures and high pressures can be quenchable to ambient conditions. Therefore, the investigation of superconductivity in carbon-based materials has always been in focus, and new discoveries continue to emerge [15–19]. For instance, multiple types of carbon-based superconductors have been confirmed, including boron-doped diamond, Q-carbon, graphite-diamond hybrid (3D carbon framework) [16–19], YbC_6 and CaC_6 (2D carbon framework) [20,21], Li_2C_2 (1D carbon form) [22], and alkali metal doped C_{60} (0D carbon form) [23,24].

Graphite intercalation compounds (GICs) are typical layered compounds formed by inserting other atoms or molecules into interlayer spaces of graphene. Generally, an n-stage GIC represents n successive graphene layers that are separated by the intercalant species [25]. At ambient pressure, some alkali metal (AM)/alkaline earth metal (AE) GICs have been synthesized, such as AMC_8 (AM = K, Rb, Cs, T_c less than 1 K) [26] and AEC_6 (AE = Ca, Sr, Ba, T_c = 11.5, 1.65, 0.065 K) [20,21,27,28]. Under high pressure, not only were GICs with higher alkali metal concentration synthesized, but the superconductivity was further improved, such as 1.9 K at 3.3 GPa for LiC_2 [29], 5 K at 3.5 GPa for NaC_2 [30], and 15.1 K at 7.5 GPa for CaC_6 [31]. It is apparent that the synthesis of AM/AE GICs could be realized at very low or even ambient pressure, which is a great advantage compared to the synthesis of hydrides. However, GIC superconductors with T_c greater than CaC_6 (11.5 K) have not been reported to date.

Indeed, the reaction of sodium with carbon at high pressures is promising and the resultant compounds have interesting crystal structures and electronic properties. It was reported that GICs NaC_2 and NaC_3 have been synthesized at pressures ranging 1.6–3.7 GPa [30]. In particular, GIC NaC_2 exhibits a measured T_c of 5.0 K at 3.5 GPa, but its crystal structure remains unresolved. Furthermore, the stable compounds Na_4C, Na_3C_2, NaC, Na_2C_3, and NaC_2 were predicted within the pressure range 1 atm–100 GPa. Strikingly, $P6/mmm$ NaC_2 owning the highest T_c among Na GICs is isostructural to MgB_2 [2] and has a predicted T_c of

*yanggc@ysu.edu.cn
†xfzhou@ysu.edu.cn

$\sim$ 42 K at 80 GPa [32]. Nonetheless, this structure is dynamically unstable at ambient pressure. Moreover, the cage-based NaC_6 and NaC_8 are both superconductors with the calculated T_c of 116 and 11 K, respectively [33,34]. All of these indicate that sodium carbides may hold great promise as low-pressure high-T_c superconductors. Meanwhile, it is unknown whether there are other Na GICs under pressure and whether they are superconducting. With these points in mind, we systematically explored potential Na-C compounds at pressures of 5 and 10 GPa, focusing on high-pressure phases.

II. COMPUTATIONAL METHODOLOGY

Crystal structure prediction has played a major role in accelerating the discovery of new materials, especially at extreme conditions [35–40]. In this work, the variable-composition evolutionary algorithm USPEX was utilized to predict thermodynamically stable compounds in the Na-C system [35,36]. At the selected pressures of 5 and 10 GPa, we performed structure searches with an unbiased sampling of the entire range of compositions, varying the stoichiometries and their structures simultaneously. Specifically, two independent structure searches at each pressure were performed with the number of atoms per primitive cell ranging 6–20 and 16–32, respectively. For each structure search, we utilized plane-wave basis sets with the cutoff of 600 eV and a grid of spacing $2\pi \times 0.06\,\text{Å}^{-1}$ for Brillouin zone (BZ) sampling. The first generation was produced randomly and the fittest 40% of the population were given the probabilities to be the parent structures in the next generation—20% by heredity, 20% by lattice mutation, 10% by transmutation, and 50% were newly added random structures. The initial population consisted of 60 structures, and all other generations combined add up to $\sim$3000 structures, thus the total number of structures is $\sim$12000 at pressures of 5 and 10 GPa. Structure relaxations and electronic properties calculations were carried out within the framework of density functional theory [41,42] as implemented by the Vienna *ab initio* simulation package (VASP) [43]. The generalized gradient approximation (GGA) of the Perdew-Burke-Ernzerhof (PBE) functional was employed for the calculation [44]. The projector augmented wave (PAW) potentials [45], with $2s^2\,2p^6\,3s^1$ and $2s^2\,2p^2$ valence electrons for Na and C atoms, were used to describe the interactions between electrons and ions. A plane wave basis set with a cutoff of 1000 eV and the k-point meshes with a resolution better than $2\pi \times 0.022\,\text{Å}^{-1}$ in the reciprocal space were used to ensure the total energy convergence (10^{-6} eV/cell). We fully relaxed the lattice parameters and atomic coordinates until the force on each atom was less than 0.001 eV/Å.

The Quantum ESPRESSO package [46] was used to calculate lattice dynamics and electron-phonon coupling (EPC) using optimized norm-conserving Vanderbilt pseudopotentials (ONCVPSP) [47]. The wave function cutoff energy was 150 Ry, and the charge density cutoff energy was 600 Ry. Different k meshes (q meshes) were chosen for the predicted compounds: $15 \times 15 \times 9$ ($5 \times 5 \times 3$) for $P2_1/m$ NaC_2, $12 \times 12 \times 12$ ($6 \times 6 \times 6$) for $Cmcm$ NaC_4, and $16 \times 16 \times 16$ ($8 \times 8 \times 8$) $P6/mmm$ NaC_6. In addition, EPC calculations were also performed for GIC CaC_6 with norm-conserving pseudopotentials. The cutoff energy of wave functions and the q mesh are adopted using 60 Ry and $6 \times 6 \times 6$, respectively. The T_c value was estimated by the Allen-Dynes-modified McMillan formula [48],

$$T_c = \frac{\omega_{\log}}{1.2} \exp\left(-\frac{1.04(1+\lambda)}{\lambda - \mu^*(1+0.62\lambda)}\right),$$

where λ is the EPC strength, $\omega_{\log}$ is the logarithmic average phonon frequency, and μ^* is the Coulomb pseudopotential parameter. The parameters λ and $\omega_{\log}$ are defined as

$$\lambda = 2\int_0^{\infty} \frac{\alpha^2F(\omega)}{\omega} d\omega,$$

and

$$\omega_{\log} = \exp\left(\frac{2}{\lambda}\int_0^{\infty} \frac{d\omega}{\omega}\alpha^2F(\omega)\ln\omega\right),$$

respectively.

III. RESULTS AND DISCUSSION

The enthalpy of formation (ΔH_f) is defined as $\Delta H_f(\mathrm{Na}_{1-x}\mathrm{C}_x) = H(\mathrm{Na}_{1-x}\mathrm{C}_x) - (1-x)H(\mathrm{Na}) - (x)H(\mathrm{C})$, where H represents the enthalpy of compounds or elemental solids. At a given pressure, the Na-C structures located on the convex hulls [indicated by solid lines in Fig. 1(a)] are thermodynamically stable against decomposition into other binary compounds and elemental solids. As illustrated in Fig. 1(a), NaC_2 with $P2_1/m$ symmetry and NaC_6 with $P6/mmm$ symmetry are thermodynamically stable at 5 GPa, which is partially consistent with the experimental results where the first-stage GIC NaC_2 and NaC_3 were synthesized below 4 GPa. At 10 GPa, NaC_4 with $Cmcm$ symmetry emerges on the convex hull, but NaC_6 is metastable. To provide more information for future experimental study, the pressure-composition phase diagram was plotted in Fig. 1(b), which demonstrates the thermodynamic stability range of the predicted compounds. Specifically, $P2_1/m$ NaC_2 is stable in the pressure ranges from 4.4 to at least 10 GPa, and 2.9–9.3 GPa for $P6/mmm$ NaC_6, whereas $Cmcm$ NaC_4 is stable above 8.9 GPa. Additional calculations including van der Waals (vdW) correction were carried out by using optB88-vdW [49]. As shown in Fig. S1 of the Supplemental Material [50], the inclusion of vdW interaction just slightly affects the stable pressure ranges of on the predicted structures. The pressure of formation for Na GICs should be easily accessible within the current experimental technology, i.e., large-volume multianvil system or diamond anvil cell experiments. What is more important, these predicted high-pressure structures may be quenchable to ambient pressure [Figs. S2(a)–S2(c) of the Supplemental Material [50]], giving them potential practical value.

As shown in Fig. 2, the three compounds demonstrate a common structural feature: the C atoms constitute the honeycomblike graphene, and the Na atoms are located within interlayer space. As a result, all of the predicted stable phases belong to the first-stage GICs. Their lattice parameters and atomic positions at 5 GPa are listed in Table S1 of the Supplemental Material [50]. $P2_1/m$ NaC_2 has a monoclinic structure, in which the Na atoms form double layers [Fig. 2(a)]. Within the Na layer, the nearest Na-Na distance is $\sim$3.28 Å.

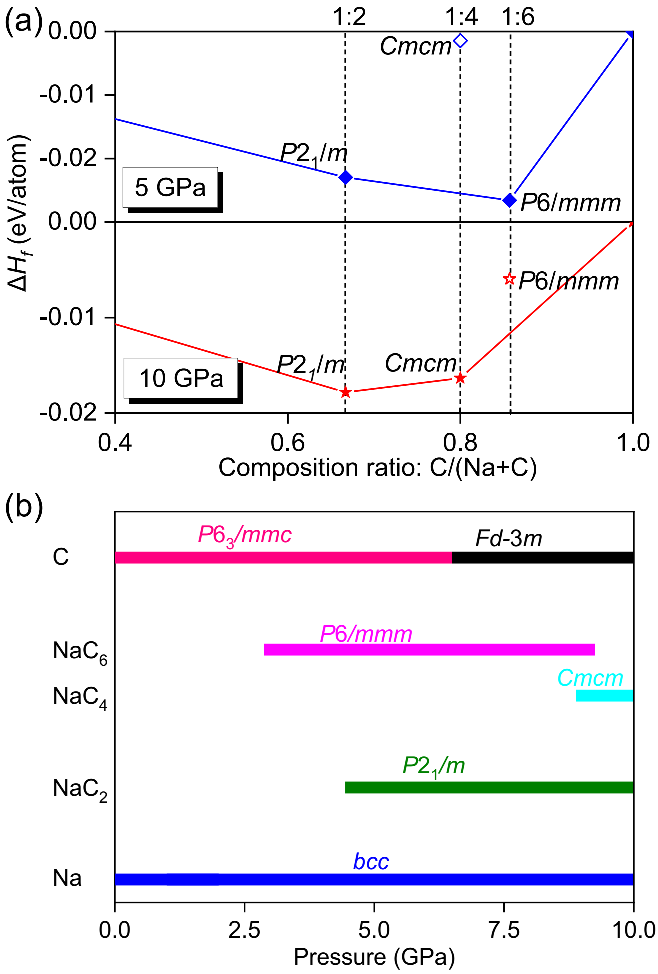

FIG. 1. (a) The calculated convex hulls for the Na-C systems at 5 and 10 GPa. The elemental reference structures are bcc Na, graphite at 5 GPa, and diamond at 10 GPa, respectively. (b) Pressure-composition phase diagram of Na-C compounds within the pressure range 0–10 GPa.

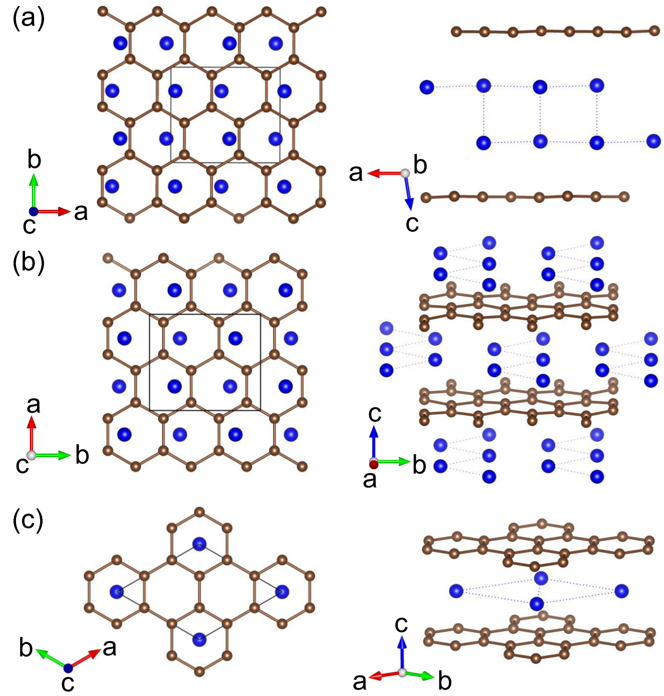

FIG. 2. Crystal structures of Na GICs at 5 GPa. (a) $P2_1/m$ NaC_2, (b) *Cmcm* NaC_4, and (c) $P6/mmm$ NaC_6. For these structures, the blue and brown spheres represent Na and C atoms, respectively.

Between the Na layers the shortest Na-Na distances are 3.21 and 3.32 Å, respectively. *Cmcm* NaC_4 has an orthorhombic structure [Fig. 2(b)] above 8.9 GPa, where the shortest Na-Na distance is ∼3.12 Å. Notably, metal atoms in GICs are usually located above the center of the hexagonal carbon ring, but Na atoms in NaC_4 are significantly displaced from the center. Here, we have constructed a hypothetical model of *c*-NaC_4 by moving the Na atoms above the center of the hexagonal carbon ring. After structure relaxation, Na atoms in *c*-NaC_4 return to the original positions of *Cmcm* NaC_4. In other words, Na atoms in *Cmcm* NaC_4 prefer to locate above the off-center configuration. $P6/mmm$ NaC_6 has Na atoms arranged in a triangular lattice with the nearest distance of ∼4.31 Å [Fig. 2(c)], similar to the B layer in $P6/mmm$ BH [51]. Moreover, the stacking sequence of graphene and Na layers in $P6/mmm$ NaC_6 is $A\alpha A\alpha$, which differs from that in *R*-3*m* CaC_6, where it is $A\alpha A\beta A\gamma A$ [52].

We examine the chemical bonding of the three Na GICs at 5 GPa by analyzing electron localization function (ELF) and Bader charges (Fig. S3 and Table S2) [50]. There is no apparent charge localization between Na and C, indicating that the Na-C bonding is not covalent. The Na-C interaction is significantly weaker than the C-C covalent interaction. As shown in Table S2, the amount of charge transfer from per Na to C atoms gradually increases with the enhancement of C content, which leads to a decrease in the green area of the Na sublattice (Fig. S3). It was noteworthy that the average charge gained per C atom is similar in NaC_4 and CaC_6. The C-C bond lengths are slightly larger than those in pristine graphene (Table S3) [50,53], which can be attributed to the transferred electrons occupying the C-C antibonding orbital, weakening the covalent C-C bond. Additionally, the shortest Na-C distance in NaC_4 is less than that of NaC_2 and NaC_6 at 5 GPa, which may lead to a distinct electronic behavior.

Inspired by the unique structures of the three predicted Na GICs, we proceeded to explore their electronic properties through calculating projected electronic band structures and density of states (DOS). The three phases demonstrate intrinsic metallicity with several bands crossing the Fermi level [E_F, Figs. 3(a) and 3(b), and Figs. S4(a)–S4(d)] [50]. The total electronic DOS at E_F are 0.27, 0.25, and 0.20 states/(eV atom) for NaC_2, NaC_4, and NaC_6 at 5 GPa, respectively. Interestingly, the E_F of NaC_4 is closest to the Van Hove singularities, implying that it may have better superconductivity [54,55]. Subsequently, we focused on analyzing the electronic properties of *Cmcm* NaC_4. At 5 GPa, its metallicity mainly arises from the C p_z orbital electrons [Fig. 3(b)], which form a system of delocalized π bonds. The delocalized π electrons in the honeycomblike graphene play a critical role in metallicity. One can notice steep bands along the *S*-*R*, *R*-*Z*, and *Z*-*T* directions and flat bands at the high symmetry points *T* and Γ

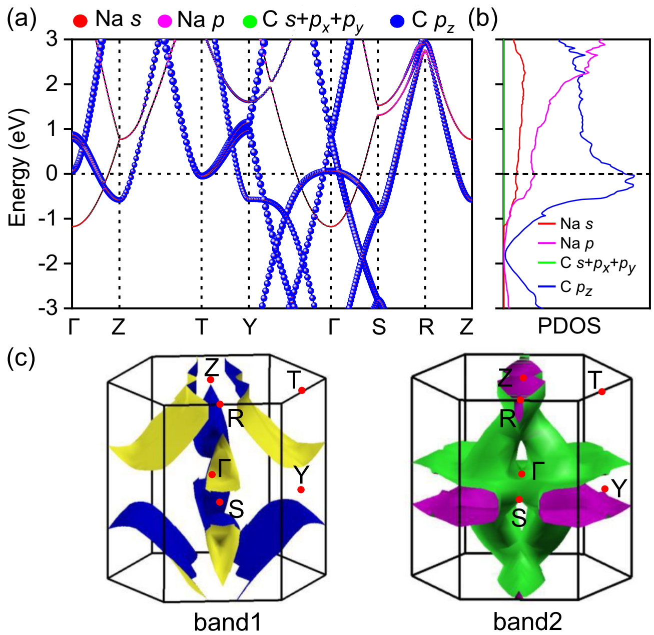

FIG. 3. (a) The orbital-resolved band structures of *Cmcm* NaC_4 at 5 GPa. (b) Projected density of states (PDOS) (the dashed line indicates E_F). (c) The Fermi surfaces associated with two bands crossing E_F.

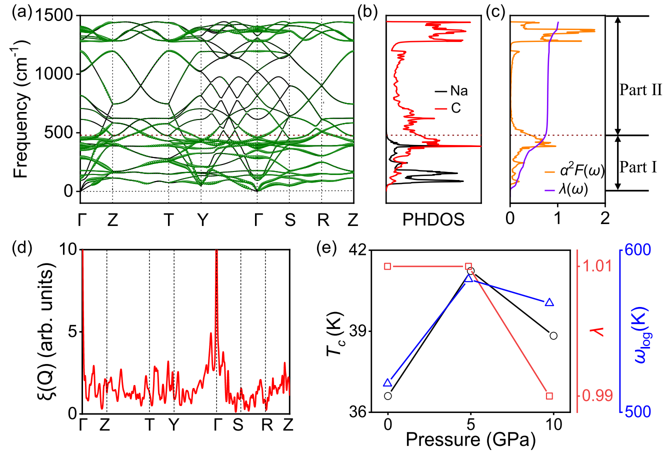

FIG. 4. (a) Phonon dispersion curves of *Cmcm* NaC_4 at 5 GPa (the magnitude of $\lambda_{q,\upsilon}$ indicated by the thickness of the green curves). (b) Projected phonon DOS (PHDOS). (c) Eliashberg spectral function $\alpha^2F(\omega)$ (orange line), frequency-dependent EPC parameter $\lambda(\omega)$ (purple line). Part I (λ_I) and part II (λ_{II}) were classified to further explore the superconductivity. (d) The Fermi surface nesting function $\xi_{\mathbf{q}}$ along some $\boldsymbol{q}$ trajectories. (e) Pressure-dependent T_c, $\omega_{\log}$, and λ of *Cmcm* NaC_4.

near E_F [Fig. 3(b)], signifying the high electron velocity and large DOS.

The topology of the Fermi surface is helpful in understanding the behavior of electrons at E_F. For *Cmcm* NaC_4, there are three bands crossing E_F [Fig. 3(c) and Fig. S5 [50]]. Here, we explore band 1 and band 2, which make the dominant contribution to the Fermi surface. The Fermi surface of band 1 consists of eight sheets, whereas band 2 is composed of one "8"-type and two U-type sheets. Apart from the minor contribution of Na p states to the Fermi surface from band 2, the two Fermi surfaces are mainly derived from the C p_z states. More interestingly, the two Fermi surfaces are nested along the body diagonal and Γ-*Z*/*S*/*Y* direction of the Brillouin zone (BZ). It is known that nesting can lead to a superconductivity or instability. It could be in favor of EPC since NaC_4 is mechanically and dynamically stable under pressure [Fig. 3(c)].

To establish the reliability of our computational method, we first employed the Allen-Dynes modified McMillan equation to estimate the superconductivity of GIC CaC_6. The calculated values of λ, $\omega_{\log}$, and T_c are 0.75, 386.9 K, and 11.3 K, respectively, with $\mu^* = 0.14$, which is in good agreement with both theoretical and experimental results [20,21,56,57]. For Na GICs, superconductivity of $P2_1/m$ NaC_2 at 3.5 GPa was also calculated with $\mu^* = 0.1$ (Fig. S6 [50]). The computed T_c of 5.4 K is in excellent agreement with the measured value of 5.0 K in NaC_2 at 3.5 GPa [30]. By contrast, the calculated EPC parameter λ of *Cmcm* NaC_4 is 1.01 at 5 GPa, comparable to MgB_2 (1.0 at 0 GPa) [58]. The phonon dispersion curves with λ weights show strong EPC in the range 0–479 and $1200-1448\,\mathrm{cm}^{-1}$ in the whole BZ [Fig. 4(a)], especially in the range $0-479\,\mathrm{cm}^{-1}$ along the Γ-*Z*, Γ-*Y*, and Γ-*S* directions. This result is mostly related to phonon softening consistent with the Fermi surface nesting, supported by the distinct sharp peaks of the Fermi surface nesting function $\xi_{\mathbf{q}}$ [Fig. 4(d)]. By comparing the Eliashberg spectral function $\alpha^2F(\omega)$ and PHDOS, we found that low frequency phonons (below $479\,\mathrm{cm}^{-1}$), associated with vibrations of Na and C atoms, contribute 69% to λ, while high-frequency phonons ($479-1448\,\mathrm{cm}^{-1}$) contribute 30% [Figs. 4(b)–4(c)]. The latter is related to vibrations of strong covalent C-C bonds. As a result, superconductivity of NaC_4 predominantly originates from the coupling of C p_z electrons with the low-frequency phonons. The estimated T_c is 41.2 K at 5 GPa with a value of $\mu^* = 0.1$, making it the highest among the reported GICs. Superconductivity of NaC_4 was investigated by us at the pressures of 0, 5, and 10 GPa [Fig. 4(e)]. At zero pressure, the estimated T_c of *Cmcm* NaC_4 is 36.6 K. With increasing pressure, T_c rises first (41.2 K at 5 GPa) and then falls (38.8 K at 10 GPa), which can be explained by the variations of $\omega_{\log}$ and λ. From 0 to 5 GPa, λ remains unchanged for *Cmcm* NaC_4, while $\omega_{\log}$ is significantly enhanced due to phonon stiffening, leading to a higher T_c value. As pressure increases from 5 to 10 GPa, both $\omega_{\log}$ and λ gradually decrease, leading to the decline of T_c.

Superconductivity of NaC_2 and NaC_6 was also analyzed and compared to that of NaC_4 at 5 GPa (Fig. S7 and Tables S4 and S5 [50]). The resulting λ values are 0.43 and 0.44 for NaC_2 and NaC_6, respectively, which are significantly lower than that of NaC_4 (1.01). The corresponding T_c values are 5.0, 41.2, and 8.3 K for NaC_2, NaC_4, and NaC_6, respectively. To understand the superior superconductivity of NaC_4 relative to NaC_2 and NaC_6, the EPC strength λ can be approximately divided into two parts: part I (λ_I) is contributed by low-frequency phonon modes associated with the vibrations of Na and C atoms, whereas part II (λ_{II}) is contributed by middle- and high-frequency phonon modes associated with

C-dominated vibrations (Fig. S7, Table S5 [50]. According to this definition, λ_I (69% of λ_{total}) plays a crucial role in the superconductivity of NaC_4 at 5 GPa, which may be related to its shorter Na-C distances. In contrast, λ_{II} dominates the superconductivity in NaC_2 and NaC_6, accounting for 65% and 86% of λ_{total}, respectively. For NaC_4, the overlap of vibrational spectra of Na and C atoms between 300 and 500 cm^{-1} [Fig. 4(b)] associated with relatively strong Na-C bond results in sharp peaks of the $\alpha^2 F(\omega)$ curves, which significantly enhances the EPC strength λ_I. Therefore, even though the carbon sublattice is similar in the three Na GICs, the difference in the concentration and configuration of Na substantially affects the EPC.

IV. CONCLUSIONS

In summary, three Na GICs, NaC_2, NaC_4, and NaC_6, were predicted in *ab initio* evolutionary structure searches. Among them, NaC_4 demonstrates a T_c of 41.2 K at 5.0 GPa. The superconductivity of NaC_4 mainly originates from the coupling of C p_z electrons with the low-frequency phonons (the vibrations of Na and C atoms), which is distinct from that of NaC_6 (the coupling of C p_z electrons with C-derived vibrations). Strikingly, the predicted T_c value of NaC_2 is very close to the measured one, suggesting that the long-lasting puzzle surrounding the structure of experimental NaC_2 may have been resolved.

ACKNOWLEDGMENTS

This work was supported by the National Key R&D Program of China (Grant No. 2022YFA1402300) and National Natural Science Foundation of China (Grants No. 52025026, No. 52090020, No. 12174200, and No. 92263101). A.R.O. acknowledges funding from Russian Science Foundation (Grant No. 19-72-30043).

[1] J. G. Bednorz and K. A. Müller, Possible high T_c superconductivity in the Ba-La-Cu-O System, Z. Phys. B **64**, 189 (1986).

[2] J. Nagamatsu, N. Nakagawa, T. Muranaka, Y. Zenitani, and J. Akimitsu, Superconductivity at 39 K in magnesium diboride, Nature (London) **410**, 63 (2001).

[3] L. Ma, K. Wang, Y. Xie, X. Yang, Y. Wang, M. Zhou, H. Liu, X. Yu, Y. Zhao, H. Wang, G. Liu, and Y. Ma, High-temperature superconducting phase in clathrate calcium hydride CaH_6 up to 215 K at a pressure of 172 GPa, Phy. Rev. Lett. **128**, 167001 (2022).

[4] N. W. Ashcroft, Metallic hydrogen: A high-temperature superconductor? Phys. Rev. Lett. **21**, 1748 (1968).

[5] N. W. Ashcroft, Hydrogen dominant metallic alloys: High temperature superconductors? Phys. Rev. Lett. **92**, 187002 (2004).

[6] P. Kong, V. S. Minkov, M. A. Kuzovnikov, A. P. Drozdov, S. P. Besedin, S. Mozaffari, L. Balicas, F. F. Balakirev, V. B. Prakapenka, S. Chariton, D. A. Knyazev, E. Greenberg, and M. I. Eremets, Potential high-T_c superconducting lanthanum and yttrium hydrides at high pressure, Nat. Commun. **12**, 5075 (2021).

[7] M. Somayazulu, M. Ahart, A. K. Mishra, Z. M. Geballe, M. Baldini, Y. Meng, V. V. Struzhkin, and R. J. Hemley, Evidence for superconductivity above 260 K in lanthanum superhydride at megabar pressures, Phys. Rev. Lett. **122**, 027001 (2019).

[8] Z. Zhang, T. Cui, M. J. Hutcheon, A. M. Shipley, H. Song, M. Du, V. Z. Kresin, D. Duan, C. J. Pickard, and Y. Yao, Design principles for high-temperature superconductors with a hydrogen-based alloy backbone at moderate pressure, Phys. Rev. Lett. **128**, 047001 (2022).

[9] X. Zhang, Y. Zhao, and G. Yang, Superconducting ternary hydrides under high pressure, WIREs Comput. Mol. Sci. **12**, e1582 (2022).

[10] W. Chen, D. V. Semenok, X. Huang, H. Shu, X. Li, D. Duan, T. Cui, and A. R. Oganov, High-temperature superconducting phases in cerium superhydride with a T_c up to 115 K below a pressure of 1 megabar, Phys. Rev. Lett. **127**, 117001 (2021).

[11] X. Liang, A. Bergara, X. Wei, X. Song, L. Wang, R. Sun, H. Liu, R. J. Hemley, L. Wang, G. Gao, and Y. Tian, Prediction of high-T_c superconductivity in ternary lanthanum borohydrides, Phys. Rev. B **104**, 134501 (2021).

[12] F. Lavini, M. Rejhon, and E. Riedo, Two- dimensional diamonds from sp^2-to-sp^3 phase transitions, Nat. Rev. Mater. **7**, 814 (2022).

[13] E. D. Miller, D. C. Nesting, and J. V. Badding, Quenchable transparent phase of carbon, Chem. Mater. **9**, 18 (1997).

[14] B. Sundqvist, Carbon under pressure, Phys. Rep. **909**, 1 (2021).

[15] H. Zhou, T. Xie, T. Taniguchi, K. Watanabe, and A. F. Young, Superconductivity in rhombohedral trilayer graphene, Nature (London) **598**, 434 (2021).

[16] E. A. Ekimov, V. A. Sidorov, E. D. Bauer, N. N. Mel'nik, N. J. Curro, J. D. Thompson, and S. M. Stishov, Superconductivity in diamond, Nature (London) **428**, 542 (2004).

[17] A. Bhaumik, R. Sachan, and J. Narayan, High-temperature superconductivity in boron-doped Q-carbon, ACS Nano **11**, 5351 (2017).

[18] A. Bhaumik, R. Sachan, S. Gupta, and J. Narayan, Discovery of high-temperature superconductivity ($T_c = 55$ K) in B-doped Q-carbon, ACS Nano **11**, 11915 (2017).

[19] Y. Ge, K. Luo, Y. Liu, G. Yang, W. Hu, B. Li, G. Gao, X.-F. Zhou, B. Xu, Z. Zhao, and Y. Tian, Superconductivity in graphite-diamond hybrid, Mater. Today Phys. **23**, 100630 (2022).

[20] T. E. Weller, M. Ellerby, S. S. Saxena, R. P. Smith, and N. T. Skipper, Superconductivity in the intercalated graphite compounds C_6Yb and C_6Ca, Nat. Phys. **1**, 39 (2005).

[21] N. Emery, C. Hérold, M. d'Astuto, V. Garcia, Ch. Bellin, J. F. Marêché, P. Lagrange, and G. Loupias, Superconductivity of bulk CaC_6, Phys. Rev. Lett. **95**, 087003 (2005).

[22] M. Gao, X. Kong, Z. Lu, and T. Xiang, First-principles study of electron-phonon coupling and superconductivity in compound Li_2C_2, Acta Phys. Sin. **64**, 214701 (2015).

[23] A. Y. Ganin, Y. Takabayashi, Y. Z. Khimyak, S. Margadonna, A. Tamai, M. J. Rosseinsky, and K. Prassides, Bulk superconductivity at 38 K in a molecular system, Nat. Mater. **7**, 367 (2008).

[24] A. F. Hebard, M. J. Rosseinsky, R. C. Haddon, D. W. Murphy, S. H. Glarum, Palstra, Thomas, A. P. Ramirez, and A. R. Kortan,

Superconductivity at 18 K in potassium-doped C_{60}, Nature (London) **350**, 600 (1991).

[25] M. S. Dresselhaus and G. Dresselhaus, Intercalation compounds of graphite, Adv. Phys. **51**, 1 (2002).

[26] N. B. Hannay, T. H. Geballe, B. T. Matthias, K. Andres, P. Schmidt, and D. MacNair, Superconductivity in graphitic compounds, Phys. Rev. Lett. **14**, 225 (1965).

[27] J. S. Kim, L. Boeri, J. R. O'Brien, F. S. Razavi, and R. K. Kremer, Superconductivity in heavy alkaline-earth intercalated graphites, Phys. Rev. Lett. **99**, 027001 (2007).

[28] S. Heguri, N. Kawade, T. Fujisawa, A. Yamaguchi, A. Sumiyama, K. Tanigaki, and M. Kobayashi, Superconductivity in the graphite intercalation compound BaC_6, Phys. Rev. Lett. **114**, 247201 (2015).

[29] I. T. Belash, A. D. Bronnikov, O. V. Zharikov, and A. V. Palnichenko, Superconductivity of graphite intercalation compound with lithium C_2Li, Solid State Commun. **69**, 921 (1989).

[30] I. T. Belash, A. D. Bronnikov, O. V. Zharikov, and A. V. Palnichenko, On the superconductivity of graphite intercalation compounds with sodium, Solid State Commun. **64**, 1445 (1987).

[31] A. Gauzzi, S. Takashima, N. Takeshita, C. Terakura, H. Takagi, N. Emery, C. Hérold, P. Lagrange, and G. Loupias, Enhancement of superconductivity and evidence of structural instability in intercalated graphite CaC_6 under high pressure, Phys. Rev. Lett. **98**, 067002 (2007).

[32] Q. Yang, K. Zhao, H. Liu, and S. Zhang, Superconductive sodium carbides with pentagon carbon at high pressures, J. Phys. Chem. Lett. **12**, 5850 (2021).

[33] S. Lu, H. Liu, I. I. Naumov, S. Meng, Y. Li, J. S. Tse, B. Yang, and R. J. Hemley, Superconductivity in dense carbon-based materials, Phys. Rev. B **93**, 104509 (2016).

[34] J.-Y. You, B. Gu, and G. Su, Superconductivity in sodium-doped T-carbon, Phys. Rev. B **101**, 184521 (2020).

[35] A. R. Oganov and C. W. Glass, Crystal structure prediction using ab initio evolutionary techniques: Principles and applications, J. Chem. Phys. **124**, 244704 (2006).

[36] A. O. Lyakhov, A. R. Oganov, H. T. Stokes, and Q. Zhu, New developments in evolutionary structure prediction algorithm USPEX, Comput. Phys. Commun. **184**, 1172 (2013).

[37] Y. Wang, J. Lv, L. Zhu, and Y. Ma, CALYPSO: A method for crystal structure prediction, Comput. Phys. Commun. **183**, 2063 (2012).

[38] C. J. Pickard and R. J. Needs, *Ab initio* random structure searching, J. Phys.: Condens. Matter **23**, 053201 (2011).

[39] S. Goedecker, Minima hopping: An efficient search method for the global minimum of the potential energy surface of complex molecular systems, J. Chem. Phys. **120**, 9911 (2004).

[40] M. Amsler and S. Goedecker, Crystal structure prediction using the minima hopping method, J. Chem. Phys. **133**, 224104 (2010).

[41] W. Kohn and L. J. Sham, Self-consistent equations including exchange and correlation effects, Phys. Rev. **140**, A1133 (1965).

[42] P. Hohenberg and W. Kohn, Inhomogeneous electron gas, Phys. Rev. **136**, B864 (1964).

[43] G. Kresse and J. Furthmüller, Efficient iterative schemes for ab initio total-energy calculations using a plane-wave basis set, Phys. Rev. B **54**, 11169 (1996).

[44] J. P. Perdew, K. Burke, and M. Ernzerhof, Generalized gradient approximation made simple, Phys. Rev. Lett. **77**, 3865 (1996).

[45] P. E. Blöchl, Projector augmented-wave method, Phys. Rev. B **50**, 17953 (1994).

[46] P. Giannozzi, S. Baroni, N. Bonini, M. Calandra, R. Car, C. Cavazzoni, D. Ceresoli, G. L. Chiarotti, M. Cococcioni, and I. Dabo, QUANTUM ESPRESSO: A modular and open-source software project for quantum simulations of materials, J. Phys.: Condens. Matter **21**, 395502 (2009).

[47] D. R. Hamann, Optimized norm-conserving Vanderbilt pseudopotentials, Phys. Rev. B **88**, 085117 (2013).

[48] P. B. Allen and R. C. Dynes, Transition temperature of strong-coupled superconductors reanalyzed, Phys. Rev. B **12**, 905 (1975).

[49] J. Klimes, D. R. Bowler, and A. Michaelides, Chemical accuracy for the van der Waals density functional, J. Phys.: Condens. Matter **22**, 022201 (2010).

[50] See Supplemental Material at http://link.aps.org/supplemental/10.1103/PhysRevB.108.214507 for additional electronic properties.

[51] C. H. Hu, A. R. Oganov, Q. Zhu, G. R. Qian, G. Frapper, A. O. Lyakhov, and H. Y. Zhou, Pressure-induced stabilization and insulator-superconductor transition of BH, Phys. Rev. Lett. **110**, 165504 (2013).

[52] N. Emery, C. Hérold, and P. Lagrange, Structural study and crystal chemistry of the first stage calcium graphite intercalation compound, J. Solid State Chem. **178**, 2947 (2005).

[53] M. F. Budyka, T. S. Zyubina, A. G. Ryabenko, S. H. Lin, and A. M. Mebel, Bond lengths and diameters of armchair single wall carbon nanotubes, Chem. Phys. Lett. **407**, 266 (2005).

[54] H. J. Choi, D. Roundy, H. Sun, M. L. Cohen, and S. G. Louie, The origin of the anomalous superconducting properties of MgB_2, Nature (London) **418**, 758 (2002).

[55] Y. Quan and W. E. Pickett, Van Hove singularities and spectral smearing in high-temperature superconducting H_3S, Phys. Rev. B **93**, 104526 (2016).

[56] M. Calandra and F. Mauri, Theoretical explanation of superconductivity in C_6Ca, Phys. Rev. Lett. **95**, 237002 (2005).

[57] W. Chen, Superconductivity at 28 K in CaB_3C_3 predicted from first-principles, J. Appl. Phys. **114**, 173906 (2013).

[58] J. M. An and W. E. Pickett, Superconductivity of MgB_2: Covalent bonds driven metallic, Phys. Rev. Lett. **86**, 4366 (2001).